Temporal evolutions of the solar wind conditions at 1 AU prior to the near-Earth X lines in the tail: Superposed epoch analysis

L. Q. Zhang, L. Dai, W. Baumjohann, A. T. Y. Lui, C. Wang, H. Rème, M. W. Dunlop

AGU PUBLICATIONS

JGR

Journal of Geophysical Research: Space Physics

RESEARCH ARTICLE
10.1002/2016JA022687

Key Points:
- Solar wind condition corresponding to near-Earth magnetotail X lines
- For events classified as SW-IMF, near-Earth X line observations in the magnetotail are preceded by ~2 h intervals of southward IMF
- For events classified as NW-IMF, the northward IMF orientation preceding near-Earth X line observations lasts ~ 40 min

Correspondence to:
L. Dai,
ldai@spaceweather.ac.cn

Citation:
Zhang, L. Q., L. Dai, W. Baumjohann, A. T. Y. Lui, C. Wang, H. Rème, and M. W. Dunlop (2016), Temporal evolutions of the solar wind conditions at 1 AU prior to the near-Earth X lines in the tail: Superposed epoch analysis, *J. Geophys. Res. Space Physics*, *121*, 7488–7496, doi:10.1002/2016JA022687.

Received 18 DEC 2015
Accepted 15 JUL 2016
Accepted article online 19 JUL 2016
Published online 3 AUG 2016

The copyright line for this article was changed on 25 JUL 2018 after original online publication

Temporal evolutions of the solar wind conditions at 1 AU prior to the near-Earth X lines in the tail: Superposed epoch analysis

L. Q. Zhang[1], L. Dai[1], W. Baumjohann[2], A. T. Y. Lui[3], C. Wang[1], H. Rème[4,5], and M. W. Dunlop[6,7]

[1]State Key Laboratory of Space Weather, National Space Science Center, Chinese Academy of Sciences, Beijing, China, [2]Space Research Institute, Austrian Academy of Sciences, Graz, Austria, [3]Applied Physics Laboratory, The Johns Hopkins University, Laurel, Maryland, USA, [4]University of Toulouse, UPS-OMP, IRAP, Toulouse, France, [5]CNRS, IRAP, BP 44346, F-31028, Toulouse, France, [6]Space Research Institute, School of Astronautics, Beihang University, Beijing, China, [7]Space Sciences Division, Rutherford Appleton Laboratory, Didcot, UK

Abstract Utilizing conjunction observations of the Geotail and ACE satellites from 1998 to 2005, we investigated the temporal evolutions of the solar wind conditions prior to the formation of X lines in the near-Earth magnetotail. We first show the statistical properties of B_z, B_y, density, and velocity of the solar wind related to the 374 tail X line events. A superposed epoch analysis is performed to study the temporal evolutions of the solar wind conditions 5 h prior to the tail X lines. The solar wind conditions for tail X lines during southward interplanetary magnetic field (IMF) (SW-IMF) and northward IMF (NW-IMF) are analyzed. The main results are as follows: (1) For events classified as SW-IMF, near-Earth X line observations in the magnetosphere are preceded by ~2 h intervals of southward IMF; (2) for events classified as NW-IMF, the northward IMF orientation preceding near-Earth X line observations lasts ~ 40 min.

1. Introduction

Magnetic reconnection governs the main mass and energy transport process from the solar wind to the Earth's magnetosphere [*Dungey*, 1961; *Akasofu*, 1980, 1981; *Wygant et al.*, 1983; *Wang et al.*, 2014; *Dai et al.*, 2015]. Reconnection X lines in the magnetotail are key to understanding the development of the global substorm process [*Akasofu et al.*, 1973; *Baker et al.*, 2002; *Baumjohann*, 2002; *Angelopoulos et al.*, 2008; *Miyashita et al.*, 2009; *Zhang et al.*, 2010, 2015a].

According to the most popular substorm model, i.e., the near-Earth neutral line (NENL) model [*Baker et al.*, 1996], the southward interplanetary magnetic field (SW-IMF) continues for about an hour and energy of the solar wind are continuously loaded into the magnetotail in the growth phase, causing the plasma sheet to stretch tailward and become thinner and thinner [*McPherron*, 1972; *Baumjohann et al.*, 1992; *Ma et al.*, 1995]. A tail X line may form once the current sheet is sufficiently thin (down to about ion gyroradius) to become unstable to waves [*Sato and Hasegawa*, 1982; *Terasawa*, 1983; *Chen et al.*, 1984; *Daughton and Karimabadi*, 2005; *Dai*, 2009].

The physical picture of tail X lines in the SW-IMF is clear. The situation of tail X lines in the northward IMF (NW-IMF), however, is less understood. *Nishida et al.* [1997] first propose that the X line in the tail could form during NW-IMF. Since then, plenty of attention has been paid on the X lines in the tail during NW-IMF [e.g., *Petrukovich et al.*, 2000, 2003; *Lavraud et al.*, 2006; *Li et al.*, 2005; *Ashour-Abdalla et al.*, 2010; *Miyashita et al.*, 2011; *Park et al.*, 2015]. However, direct observational evidence of X lines during NW-IMF has not been found till the recent study of *Zhang et al.* [2015a].

According to *Zhang et al.* [2015a], X lines in the tail can occur for SW-IMF as well as NW-IMF but more frequently for SW-IMF. In particular, typical a case presented in *Zhang et al.* [2015a] clearly showed that a near-Earth X line for NW-IMF occurs while the geomagnetic activity is particularly quiet (*AE* index is about 60 nT). This is quite different from the situation of SW-IMF in which X lines are always present during enhanced geomagnetic activities [*Nagai et al.*, 1998; *Nakamura et al.*, 2001a, 2001b; *Lyons et al.*, 2012; *Zhang et al.*, 2015b]. The remnant energy in the preceding SW-IMF interval is suggested to be responsible for X lines during NW-IMF [*Peng et al.*, 2013].

It is generally understood that solar wind conditions are related to the formation of tail X line through the energy loading/unloading in the magnetotail. Southward IMF corresponds to an accumulation of energy in the magnetotail. Formation of tail X lines signals the energy unloading in the magnetotail. Still, important details of this loading/unloading process remain to be explored. In this study, we are particularly interested in two timescales of the energy loading/unloading process. In the SW-IMF, we are interested in the timescale of continuous SW-IMF needed to form a tail X line. This energy loading timescale may be related to the growth phase of substorm, which is inferred to be about 1 h [e.g., *Baker et al*., 1996]. In the NW-IMF, the formation of near-Earth tail X lines is generally expected to consume the remaining energy in the preceding SW-IMF interval. The timescale of interest in the NW-IMF is the time for tail X lines to consume the remaining energy in the near-Earth tail. Until now, knowledge of these two timescales has been from modeling or inference. Observation studies of solar wind conditions corresponding to tail X lines have not been reported so far.

In this paper, we investigate the solar wind conditions corresponding to tail X lines with statistical data from Geotail and ACE. The apogee (~30 R_E) of Geotail is well suited to observe the near-Earth tail X lines, which are generally thought to occur at 20–30 R_E. ACE continuously monitors the solar wind in the upstream. The combination of these two data sets is well suited for the subject. The organization of the paper is as follows. In section 2, we introduce the data set used in this study. In section 3, we illustrate the method to use an IMF-index to characterize the IMF orientation for tail X line events. In section 4, we show the statistical properties of B_z, B_y, density, and velocity of the solar wind related to the tail X line events. Section 5 shows the superposed epoch analysis of the solar wind conditions 5 h before the tail X line for SW-IMF and NW-IMF. In section 6, we discuss the main results in this paper. The conclusions are also included.

2. Data Descriptions

The ACE satellite is located at the L1 point between the Sun and Earth (~220 R_E from the Earth with R_E being Earth radius). The 1 min resolution solar wind ion data from Solar Wind Electron Proton Alpha Monitor [*McComas et al*., 1998] and 16 s resolution magnetic field data acquired by Magnetic field experiment [*Smith et al*., 1998] on the ACE satellite are collected from 1998 to 2005.

The 3 s resolution data from Geotail magnetometer [*Kokubun et al*., 1994] and the 12 s resolution data from the low-energy particle (LEP) instrument [*Mukai et al*., 1994] have been collected in the same interval from1998 to 2005 as ACE satellite. The LEP data on Geotail cover the energy range of several eV to 43 keV.

Signals of the X lines are identified by the tailward fast flows (TFFs) with negative B_z (refer to *Zhang et al*. [2015a]). The selection criterion of the X lines (GSM coordinates) is that the duration of $V_x < -300$ km/s exceeds 35 s and $B_z < 0$. This selection criterion is the same as the one used in *Zhang et al*. [2015a]. There are 374 X line events selected inside the region of $-30\,R_E < X < -15\,R_E$, $-10\,R_E < Y < 10\,R_E$, and $-5\,R_E < Z < 5\,R_E$.

3. IMF Conditions of the X Lines

The measurement of IMF at ACE is a L1. There is a transport time (t_{TT}) for the solar wind magnetic field to convect from L1 to the magnetopause. In addition, there is another "action time" (t_{AP}) for the solar wind IMF conditions at magnetopause to affect the X lines in the tail. These two parameters need to be considered when determining the IMF condition for the X lines in the tail. In our previous study [*Zhang et al*., 2015a], a simple method (referred to as Method1 hereinafter) is adopted to determine the direction and magnitude of the IMF B_z corresponding to X lines in the tail. In this paper, we improve the method to determine the IMF conditions for tail X lines.

A simple cartoon in Figure 1 is shown to illustrate how to determine the IMF condition of an X line in the tail. In *Zhang et al*. [2015a], the t_{TT} was assumed to be 60 min for every event. However, the real t_{TT} varies with the solar wind velocity. The solar wind velocity changes in a wide range from 250 km/s to above 800 km/s. In addition, the location X of the ACE (GSM coordinates) repeatedly varied between 215 R_E and 245 R_E in the years 1998 to 2005. Apparently, t_{TT} could be greatly different from case to case. Rather than 50 min, a more accurate estimate of the transport time t_{TT} would be based on the solar wind velocity for each event.

Another potential caveat in the previous method is the way of defining the orientation of IMF by the average value of IMF B_z. For instance, a 30 min IMF consisting of 20 min -1 nT B_z and 10 min 2.5 nT B_z was to be defined as NW-IMF in the previous method. However, such interval is more appropriately identified as

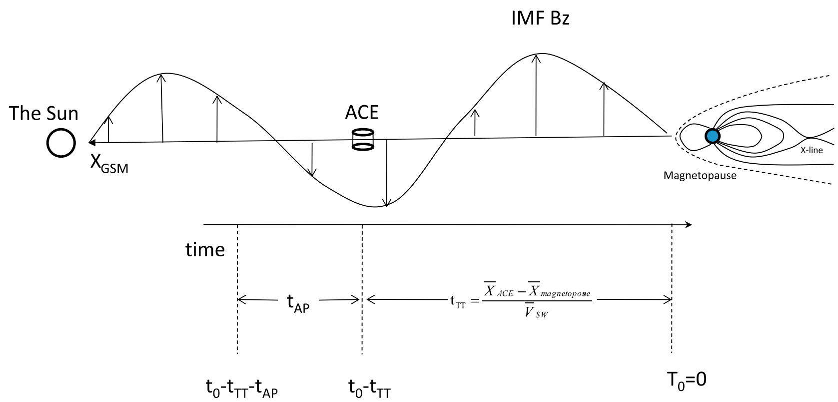

Figure 1. Cartoon of the transport of the IMF B_z that corresponds to X lines in the magnetotail. t_0 is the time for the observation of X line in the near-Earth tail. t_{TT} is the transport time from ACE to the magnetopause. t_{AP} is the action time, explained in the text. The vertical arrows in the plot denote the possible distribution of the IMF B_z.

SW-IMF-dominated interval. An equally possible case is a 30 min IMF consisting of 20 min 1 nT B_z and 10 min -2.5 nT B_z was defined as a SW-IMF. To obviate such concerns, we use an IMF-index, which is the proportion of SW-IMF data points in the total 30 min interval, to quantitatively characterize the IMF orientations. A SW-IMF-dominated interval has an IMF-index close to unity. The IMF-index is close to 0 for NW-IMF-dominated interval.

In this study, we determine the IMF B_z for each tail X line event as follows. First, for an X line at time $= t_0$ (t_0 is the time of the X line observed by the Geotail), the transport time from ACE to magnetopause t_{TT} is evaluated by $t_{TT} = \frac{X_{ACE} - X_{MP}}{V_{SW}}$, where the X_{MP} represents the location of the Earth's magnetopause (GSM coordinates). X_{MP} is chosen to be 10 R_E in this study. The X_{ACE} is the average location of ACE in the interval of t_0-50 min-30 min to t_0-50 min, while the V_{SW} is the average $|V_x|$ of the solar wind in the same interval. Here the value of 50 min is the most probability of the t_{TT} (as showed below), and 30 min is an appropriate timescale for average. The solar wind speed changes very little in each event. As a result, t_{TT} is very insensitive to interval over which the average solar wind speed is obtained. The distribution of t_{TT} for all events is shown in Figure 2. For most events, the transport time is close to ~50 min, corresponding to an average solar wind speed of 400 km/s.

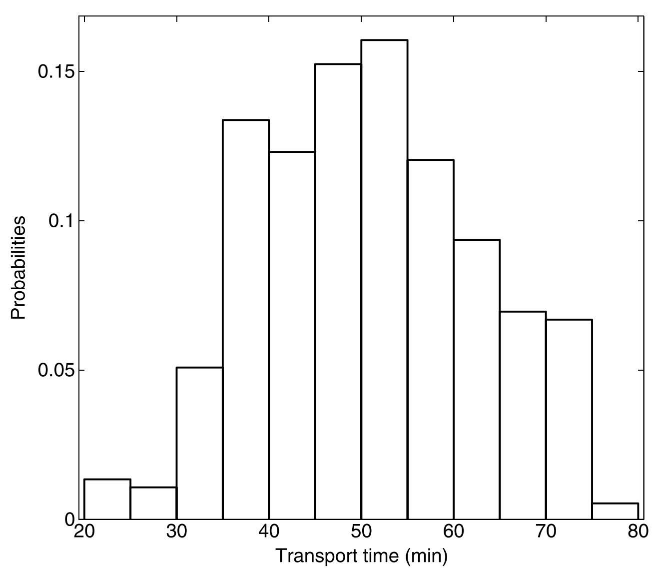

Figure 2. Distributions of the transport time (t_{TT}) from the ACE satellite to the Earth's magnetopause.

We then obtain the IMF-index for each tail X line event using the 16 s cadence magnetic field data from ACE. The IMF-index is defined as the percentage of SW-IMF data points in the interval from t_0-t_{TT}-t_{AP} to t_0-t_{TT}. The t_{TT} is calculated case by case. Here the t_{AP} is named action time. The interval t_0-t_{TT}-t_{AP} to t_0-t_{TT} corresponds to a solar wind that is shifted to the magnetopause and has a duration of t_{AP} before the observation of X lines. Roughly speaking, the "action" of this interval (t_0-t_{TT}-t_{AP} to t_0-t_{TT}) of solar wind at the magnetopause appears to lead to the result (X lines) in the tail. An order of magnitude estimate of t_{AP} may be about the timescale for reconnected field lines to convect from at dayside to the tail lobe, for instance, 15 min in MHD modeling results [e.g., *Tang et al.*, 2011; *Wang et al.*, 2014]. In real observations, there might be ~±10 min

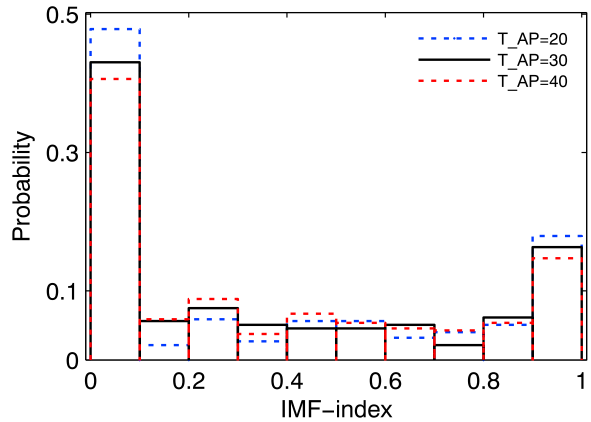

Figure 3. Distributions of the IMF-index with different t_{AP}. Three cases of t_{AP} are considered.

uncertainty. To obviate concerns on this uncertainty, we compare the IMF-index using different action time t_{AP}. In Figure 3, we plot the distribution of IMF-index with different values of t_{AP} = 20 min, 30 min, and 40 min to check the impact of its uncertainty on the IMF-index. The distributions of the IMF-index for three cases of t_{AP} are similar. The IMF for each X line is categorized as SW-IMF/NW-IMF if the IMF-index is above/less than 0.5. In our database, there are a total of 248 events for SW-IMF and 126 events for NW-IMF. This is close to the result of method of *Zhang et al.* [2015a] in which there are 251 events for SW-IMF and 123 events for NW-IMF.

4. Statistical Properties of Solar Wind Corresponding to Tail X Lines

In this section, we investigate the statistical properties of the solar wind corresponding to the 374 tail X line events. Figure 4 shows the distribution of the IMF B_z and IMF B_y of the solar wind corresponding to tail X lines. For comparison, the absolute value of IMF B_z is used for SW-IMF. The distribution shows a major peak of IMF B_z at 2 nT ~ 3 nT for SW-IMF, and ~ 2 nT for NW-IMF. Most observed tail X line events during NW-IMF intervals occur for B_z less than 4 nT. The X line during SW-IMF interval has much wider distribution of B_z from 1 nT to 6 nT with respect to NW-IMF. For both NW-IMF and SW-IMF conditions, the distribution of B_y component has a broad peak around 0, indicating that the solar wind leading to tail X lines are mostly dawn-dusk symmetric. In contrast, the tail X lines during SW-IMF intervals are more likely to occur for dawnward IMF B_y, while the tail X lines during NW-IMF intervals are more likely to occur for duskward IMF B_y. The dependences of the tail magnetic reconnections on the IMF B_y could be different for NW-IMF and SW-IMF.

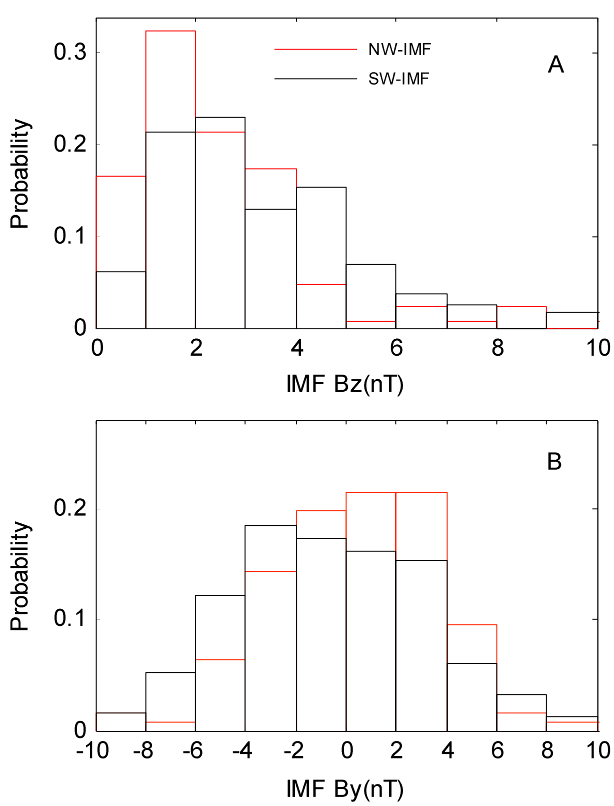

Figure 4. (a) Distributions of the tail X line-related IMF B_z. (b) Distributions of the tail X line-related IMF B_y.

Figure 5 shows the distributions of the speed, density, and the associated E_y of the solar wind related to tail X lines. For comparison, the same distribution of parameters of the background solar wind (5 h prior to the X line) is also presented. As shown in Figure 5, both speeds of the solar wind mainly distributed at lower range of 400–550 km/s. A small portion of X lines corresponds to fast solar wind of 600–700 km/s. Both peaks of the density distributions are around 3–4 cm^{-3}. The distribution of E_y is related to the double-peak distribution of B_z, with two peaks around

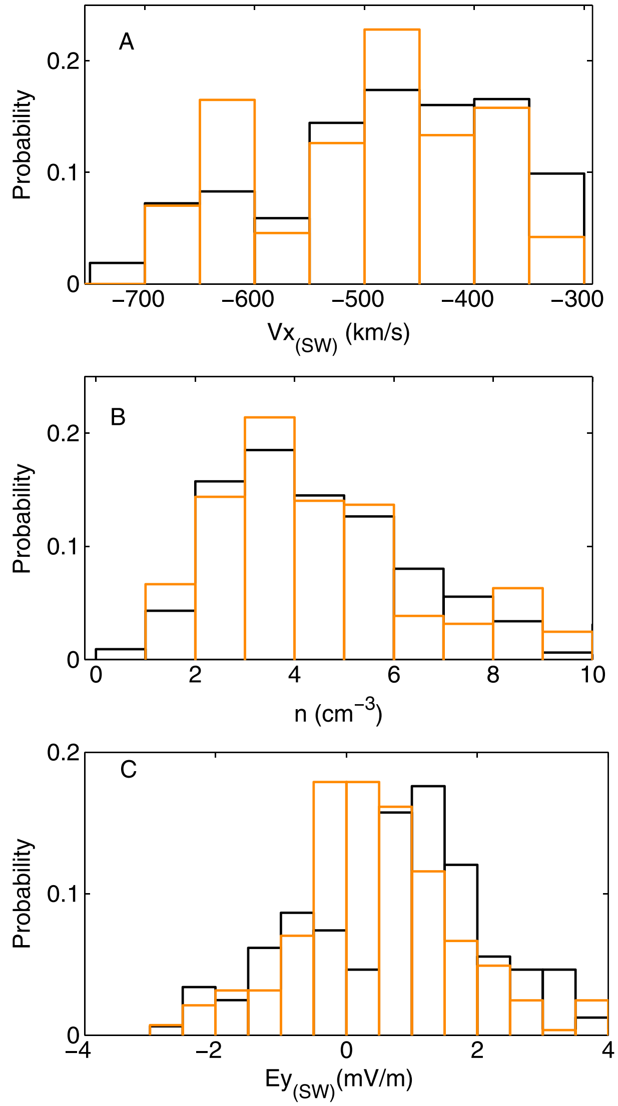

Figure 5. Distributions of the parameters of the tail X line-related solar wind. The black (orange) curve corresponds to probability in the t_{AP} (background solar wind, 5 h prior to the X lines).

+1 mV/m and −1 mV/m for X line-related solar wind condition. Distinctly different, the background solar wind is characteristic of the single peak around zero. Thus, the tail X line tends to occur at higher E_y for both NW-IMF and SW-IMF.

As shown in Figure 4a and closely related Figure 5c, although the distribution of IMF B_z in the general solar wind has a sharp peak at $B_z = 0$, the distributions of B_z for the tail X line-related events have peaks at 1–2 nT for both B_z polarities which are consistent with the observed E_y of the solar wind in Figure 5c. For southward IMF, this is a natural result as depicted in the open magnetosphere model of *Dungey* [1961] and the NENL substorm model of *Baker et al.* [1996]. For northward IMF, the larger B_z (or E_y) implies that B_z (E_y) and the corresponding Poynting flux $B_z \times E_y$ of solar wind may lead to the entry of more energy into the magnetosphere. The entry of solar wind energy could be a significant part contributed to the formation of the X lines in the tail in addition to the remnant energy during the preexisting southward IMF [*Miyashita et al.*, 2011].

5. Superposed Epoch Analyses

We performed superposed epoch analyses of the solar wind conditions at ACE 5 h prior to the X lines in the tail. In this analysis, tail X lines are identified by TFFs with negative B_z in the Geotail database. Most TFFs in our database should be generated by the near-Earth X line. Still, small amount of TFF may have propagated from X lines, not X lines themselves. The propagation time from the near-Earth X line to Geotail can be several minutes for some events. This timescale may not affect the present results based on 5 min resolution analysis.

The solar wind parameters examined include the IMF B_z components, solar wind dawn-dusk electric field (E_y, calculated by $V_x \times B_z$), the absolute value of IMF B_y, and the clock angle (calculated by arctan(IMF B_y/IMF $|B_z|$)). The X lines during NW-IMF and SW-IMF are analyzed independently. $T = 0$ is set asT_0-T_{tt}, where T_0 is the time when the tail X lines are observed by Geotail and T_{tt} is the time to transport the solar wind from ACE to the magnetopause. The interval of $t = 0$ to −300 min is divided into small bins of 5 min. Physical parameters are averaged over 5 min bins.

Figure 6 shows the superposed epoch analysis of the solar wind conditions for tail X line events corresponding to SW-IMF (IMF-index larger than 0.5).To properly display the scale of IMF near 0, Figure 6a only shows the curve of the average value of all events. Figure 6 shows the data of all profiles (thin lines) and the average profile (heavy line). The IMF B_z is first small and negative before $t = -120$ min. In the interval of $t = -120$ min to −50 min, the absolute value of the IMF B_z increases with time. The interval $t = -120$ min to −50 min is SW-

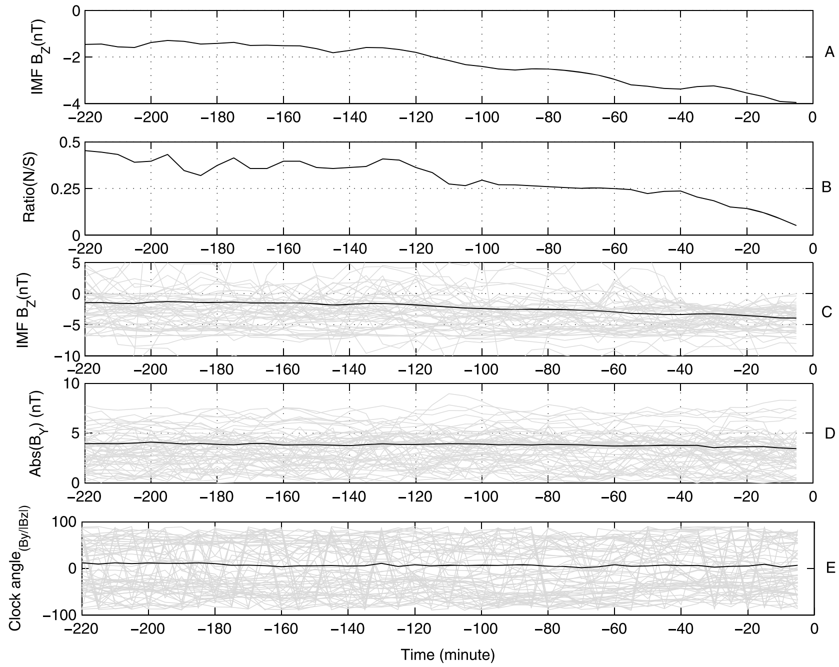

Figure 6. The temporal evolution of the tail X line-related solar wind: SW-IMF cases. $T = 0$ is set as T_0-T_{tt}, where T_0 is the time when the tail X lines are observed by Geotail and T_{tt} is the time to transport the solar wind from ACE to the magnetopause. (a) The temporal evolution of averaged IMF B_z. (b) The ratio of the $+B_z$ events to $-B_z$ events at a particular time. (c) The spread of the profiles is by thin lines, and the average value is by a heavy line. (d and e) The absolute value of IMF B_y and clock angle.

IMF dominant. After $T = -50$ min, the absolute value of the IMF B_z has a more rapid increase. Hence, X lines in the tail correspond to a moderate enhancement of southward IMF B_z from $t = -120$ min to 0 min. Figure 6b shows the ratio of $+B_z/-B_z$ event at a particular time. The ratio of $+B_z/-B_z$ event is an index defined for events at each time bin. If the IMF B_z at a time bin is positive for one event, then we add one count of $+B_z$ event for that time bin. If the IMF B_z is negative at a time bin for one event, then we add one count of $-B_z$ event for that time bin. When a very negative B_z event combined with many small positive $+B_z$ events, the overall result may be a negative B_z in superposed epoch analysis. But such a final result may be difficult to interpret. From the ratio of $+B_z/-B_z$ event, we confirmed that an average negative B_z indeed corresponds to a dominant portion of $-B_z$ events. The ratio $+B_z/-B_z$ was smaller than 0.3 from $t = -120$ min to 0 min. From Figure 6c, an average negative $-B_z$ indeed corresponds to a dominant portion of $-B_z$ events. This gives more statistical confidence on our superposed epoch analysis results. Both the average B_z and the ratio of $+B_z/-B_z$ events indicate that the SW-IMF is dominant from $t = -120$ min to 0 min. The SW-IMF period X line appears to correspond to a moderate SW-IMF lasting for 120 min on the average.

Figure 7 shows the superposed epoch analysis of the solar wind condition for X line events corresponding to the NW-IMF. Same as in the analysis of Figure 6, $t = 0$ is set as T_0-T_{tt}. From $t = -220$ min to -50 min, the mean IMF B_z slightly varies between positive and negative. As shown in Figure 7b, the ratio of $+B_z/-B_z$ events is quite stable and very close to unity. The SW-IMF is dominant from $t = -220$ min to -50 min. Thus, a weak SW-IMF appears to precede the NW-IMF for the tail X lines. The IMF B_z is dominantly northward from $t = -40$ min to $t = 0$ min. This is clearly seen in the superpose epoch analysis and also in the ratio of $+B_z/-B_z$ event. From $t = -50$ min to $t = -40$ min, the ratio of N/S in Figure 7b begins to increase with time. Accordingly, the absolute value of IMF B_z increases to become positive.

Prolonged intervals of an unchanged IMF B_z polarity are frequent in the solar wind. An interesting issue is if the mean profiles shown in Figures 6 and 7 are different from a randomly selected background solar wind. We analyzed the temporal evolution of a randomly selected background solar wind condition in the years 2000 and 2001. We take first 6 h of each day of 1 year and plot the equivalents of Figures 6 and 7. The profiles

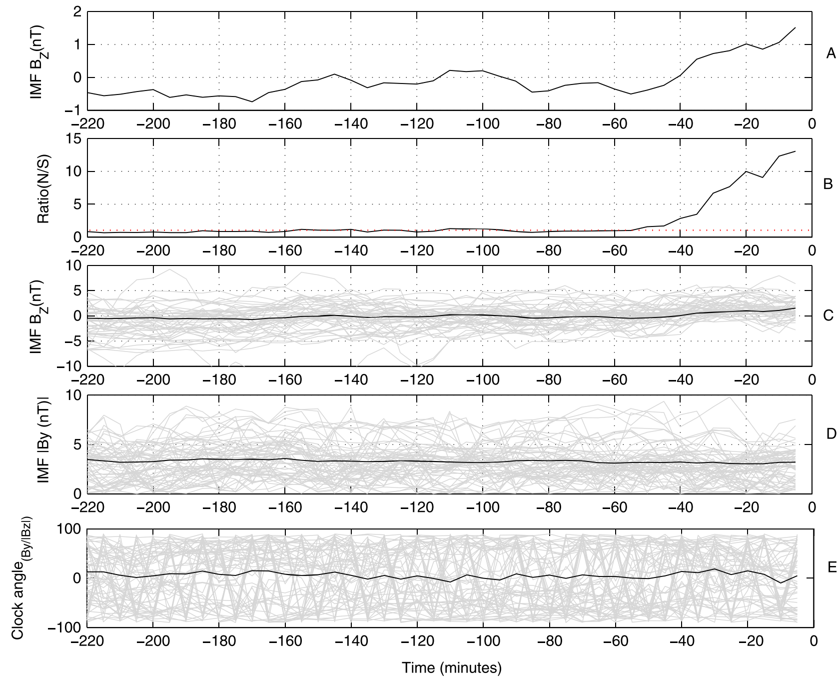

Figure 7. The temporal evolution of the tail X line-related solar wind: NW-IMF cases. The format is the same as in Figure 6.

of the randomly selected solar wind are significantly different from those associated with the X lines in our study. This blind test provides us more confidence on our results.

An interesting question is the role of IMF B_y for tail X lines related to northward IMF. Dayside reconnection occurs even if $|B_y| > B_z > 0$ [*Freeman et al.*, 1993; *Senior et al.*, 2002]. The superposed epoch analysis of B_y and clock angle are shown in Figures 7d and 7e. The value of B_y and clock angles are not particular stronger for X lines during northward IMF. Such B_y and clock angle may not be very efficient in facilitating component reconnection at dayside. But the presence of some amount of B_y may allow dragging high-latitude-reconnected magnetic field lines antisunward to the tail lobe [*Gosling et al.*, 1991; *Park et al.*, 2015].

6. Discussions and Conclusion

Solar wind conditions are related to the formation of tail X line through the energy loading/unloading in the magnetotail. Formation of tail X lines signals the energy unloading in the magnetotail. In this paper, we presented a detailed statistical study of the solar wind conditions prior to the formation of near-Earth X lines in the magnetotail. Our results of superposed epoch analysis show that on average, formation of near-Earth tail X line related to SW-IMF corresponds to a moderate 2 h (120 min) negative IMF B_z. This 2 h timescale may be related to the energy-loading phase of substorm because near-Earth X lines are generally considered as an important element in the substorm cycle.

Event studies show that small substorms can occur during NW-IMF [e.g., *Petrukovich et al.*, 2000; *Pulkkinen et al.*, 2007; *Lee et al.*, 2010; *Miyashita et al.*, 2011]. However, their strengths are distinctly weaker than that during SW-IMF [*Peng et al.*, 2013]. Consistently, the X line-related geomagnetic activities are also weaker for NW-IMF than SW-IMF [*Zhang et al.*, 2015a]. As we have known, the fractional amount of solar wind energy input into the magnetosphere during intervals of intense and long-duration NW-IMF is quite low [*Kullen and Karlsson*, 2004; *Li et al.*, 2008]. According to *Tsurutani and Gonzalez* [1995], the energy input during northward IMF could be 100 to 30 times less than during periods of intense southward IMF. The remnant energy in the preceding SW-IMF interval has been proposed to be the main energy provider [*Du et al.*, 2011; *Peng et al.*, 2013].

Our statistical study confirmed that occurrence of tail X lines may correspond to NW-IMF. Particularly, our superposed epoch analysis shows that the X line is formed within 40 min after the IMF turning northward.

This observation fact is consistent with the scenario that magnetotail energy reserved by the preceding SW-IMF is consumed within 40 min after the IMF turning northward.

The conclusions are as follows: (1) on average, formation of tail X lines related to SW-IMF corresponds to ~ 2 h moderate $-B_z$ and (2) occurrence of tail X lines may correspond to NW-IMF. Tail X lines related to NW-IMF on average occur within 40 min since northward turning of IMF.

Acknowledgments
We would like to thank the PIs and those who contributed to the success of the ACE and Geotail mission. The data of ACE and Geotail satellites are available from http://cdaweb.gsfc.nasa.gov. This study is supported by the National Natural Science Foundation of China (41231067, 41574161, and 41374188) and in part by the specialized research fund for state key laboratories.

References

Akasofu, S.-I. (1980), The solar wind-magnetosphere energy coupling and magnetospheric disturbances, *Planet. Space Sci.*, *28*, 495–509, doi:10.1016/0032-0633(80)90031-8.

Akasofu, S.-I. (1981), Energy coupling between the solar wind and the magnetosphere, *Space Sci. Rev.*, *28*, 121–190, doi:10.1007/BF00218810.

Akasofu, S.-I., P. D. Perreault, F. Yasuhara, and C.-I. Meng (1973), Auroral substorms and the interplanetary magnetic field, *J. Geophys. Res.*, *78*(31), 7490–7508, doi:10.1029/JA078i031p07490.

Angelopoulos, V., et al. (2008), Tail reconnection triggering substorm onset, *Science*, *321*(5891), 931–935, doi:10.1126/science.1160495.

Ashour-Abdalla, M., J. M. Bosqued, M. El-Alaoui, V. Peroomian, and R. Walker (2010), Observations and simulations of a highly structured plasma sheet during northward IMF, *J. Geophys. Res.*, *115*, A10227, doi:10.1029/2009JA015135.

Baker, D. N., T. I. Pulkkinen, V. Angelopoulos, W. Baumjohann, and R. L. McPherron (1996), Neutral line model of substorms: Past results and present view, *J. Geophys. Res.*, *101*(A6), 12,975–13,010, doi:10.1029/95JA03753.

Baker, D. N., et al. (2002), Timing of magnetic reconnection initiation during a global magnetospheric substorm onset, *Geophys. Res. Lett.*, *29*(24), 2190, doi:10.1029/2002GL015539.

Baumjohann, W. (2002), Modes of convection in the magnetotail, *Phys. Plasmas*, *9*, 3665–3667, doi:10.1063/1.1499116.

Baumjohann, W., G. Paschmann, and T. Nagai (1992), Thinning and expansion of the substorm plasma sheet, *J. Geophys. Res.*, *97*, 17,173–17,175, doi:10.1029/92JA01519.

Chen, J., P. J. Palmadesso, J. A. Fedder, and J. G. Lyon (1984), Fast collisionless tearing in an anisotropic neutral sheet, *Geophys. Res. Lett.*, *11*, 12–15, doi:10.1029/GL011i001p00012.

Dai, L. (2009), Collisionless magnetic reconnection via Alfven eigenmodes, *Phys. Rev. Lett.*, *102*(24), 245003, doi:10.1103/PhysRevLett.102.24500.

Dai, L., C. Wang, V. Angelopoulos, and K.-H. Glassmeier (2015), In situ evidence of breaking the ion frozen-in condition via the non-gyrotropic pressure effect in magnetic reconnection, *Ann. Geophys.*, *33*(9), 1147–1153, doi:10.5194/angeo-33-1147-2015.

Daughton, W., and H. Karimabadi (2005), Kinetic theory of collisionless tearing at the magnetopause, *J. Geophys. Res.*, *110*, A03217, doi:10.1029/2004JA010751.

Du, A. M., B. T. Tsurutani, and W. Sun (2011), Solar wind energy input during prolonged, intense northward interplanetary magnetic fields: A new coupling function, *J. Geophys. Res.*, *116*, A12215, doi:10.1029/2011JA016718.

Dungey, J. W. (1961), Interplanetary magnetic fields and the auroral zones, *Phys. Rev. Lett.*, *6*, 47–48, doi:10.1103/PhysRevLett.6.47.

Freeman, M. P., C. J. Farrugia, L. F. Burlaga, M. R. Hairston, M. E. Greenspan, J. M. Ruohoniemi, and R. P. Lepping (1993), The interaction of a magnetic cloud with the Earth: Ionospheric convection in the Northern and Southern Hemispheres for a wide range of quasi-steady interplanetary magnetic field conditions, *J. Geophys. Res.*, *98*(A5), 7633–7655, doi:10.1029/92JA02350.

Gosling, J. T., M. F. Thomsen, S. J. Bame, R. C. Elphic, and C. T. Russell (1991), Observations of reconnection of interplanetary and lobe magnetic field lines at the high-latitude magnetopause, *J. Geophys. Res.*, *96*(A8), 14,097–14,106, doi:10.1029/91JA01139.

Kokubun, S., T. Yamamoto, M. H. Acuna, K. Hayashi, K. Shiokawa, and H. Kawano (1994), The Geotail magnetic field experiment, *J. Geomagn. Geoelectr.*, *46*, 7–21, doi:10.5636/jgg.46.7.

Kullen, A., and T. Karlsson (2004), On the relation between solar wind, pseudobreakups, and substorms, *J. Geophys. Res.*, *109*, A12218, doi:10.1029/2004JA010488.

Lavraud, B., M. F. Thomsen, B. Lefebvre, S. J. Schwartz, K. Seki, T. D. Phan, Y. L. Wang, A. Fazakerley, H. Rème, and A. Balogh (2006), Evidence for newly closed magnetosheath field lines at the dayside magnetopause under northward IMF, *J. Geophys. Res.*, *111*, A05211, doi:10.1029/2005JA011266.

Lee, D.-Y., K.-C. Choi, S. Ohtani, J. H. Lee, K. C. Kim, K. S. Park, and K.-H. Kim (2010), Can intense substorms occur under northward IMF conditions?, *J. Geophys. Res.*, *115*, A01211, doi:10.1029/2009JA014480.

Li, W., J. Raeder, J. Dorelli, M. Øieroset, and T. D. Phan (2005), Plasma sheet formation during long period of northward IMF, *Geophys. Res. Lett.*, *32*, L12S08, doi:10.1029/2004GL021524.

Li, W., J. Raeder, M. F. Thomsen, and B. Lavraud (2008), Solar wind plasma entry into the magnetosphere under northward IMF conditions, *J. Geophys. Res.*, *113*, A04204, doi:10.1029/2007JA012604.

Lyons, L. R., Y. Nishimura, X. Xing, A. Runov, V. Angelopoulos, E. Donovan, and T. Kikuchi (2012), Coupling of dipolarization front flow bursts to substorm expansion phase phenomena within the magnetosphere and ionosphere, *J. Geophys. Res.*, *117*, A02212, doi:10.1029/2011JA017265.

Ma, Z. W., X. G. Wang, and A. Bhattacharjee (1995), Growth, sudden enhancement, and relaxation of current sheets in the magnetotail: Two-dimensional substorm dynamics, *Geophys. Res. Lett.*, *22*, 2985–2988, doi:10.1029/95GL02937.

McComas, D. J., S. J. Bame, P. Barker, W. C. Feldman, J. L. Phillips, and P. Riley (1998), Solar Wind Electron Proton Alpha Monitor (SWEPAM) for the advanced composition explorer, *Space Sci. Rev.*, *86*, 563–612, doi:10.1023/A:1005040232597.

McPherron, R. L. (1972), Substorm related changes in the geomagnetic tail: The growth phase, *Planet. Space Sci.*, *20*, 1521–1539, doi:10.1016/0032-0633(72)90054-2.

Miyashita, Y., et al. (2009), A state-of-the-art picture of substorm-associated evolution of the near-Earth magnetotail obtained from superposed epoch analysis, *J. Geophys. Res.*, *114*, A01211, doi:10.1029/2008JA013225.

Miyashita, Y., Y. Kamide, K. Liou, C.-C. Wu, A. Ieda, N. Nishitani, S. Machida, Y. Saito, and T. Mukai (2011), Successive substorm expansions during a period of prolonged northward interplanetary magnetic field, *J. Geophys. Res.*, *116*, A09221, doi:10.1029/2011JA016719.

Mukai, T., S. Machida, Y. Saito, M. Hirahara, T. Terasawa, N. Kaya, T. Obara, M. Ejiri, and A. Nishida (1994), The low energy particle (LEP) experiment onboard the Geotail satellite, *J. Geomagn. Geoelectr.*, *46*, 669–692, doi:10.5636/jgg.46.669.

Nagai, T., M. Fujimoto, Y. Saito, S. Machida, T. Terasawa, R. Nakamura, T. Yamamoto, T. Mukai, A. Nishida, and S. Kokubun (1998), Structure and dynamics of magnetic reconnection for substorm onsets with Geotail observations, *J. Geophys. Res.*, *103*, 4419–4440, doi:10.1029/97JA02190.

Nakamura, R., W. Baumjohann, R. Schödel, M. Brittnacher, V. A. Sergeev, M. Kubyshkina, T. Mukai, and K. Liou (2001a), Earthward flow bursts, auroral streamers, and small expansions, *J. Geophys. Res.*, *106*(A6), 10,791–10,802, doi:10.1029/2000JA000306.

Nakamura, R., W. Baumjohann, M. Brittnacher, V. A. Sergeev, M. Kubyshkina, T. Mukai, and K. Liou (2001b), Flow bursts and auroral activations: Onset timing and foot point location, *J. Geophys. Res.*, *106*(A6), 10,777–10,789, doi:10.1029/2000JA000249.

Nishida, A., T. Mukai, T. Yamamoto, Y. Saito, S. Kokubun, and R. P. Lepping (1997), Traversal of the nightside magnetosphere at 10 to 15 *Re* during northward IMF, *Geophys. Res. Lett.*, *15*, 939–942, doi:10.1029/97GL00219.

Park, K. S., D.-Y. Lee, T. Ogino, and D. H. Lee (2015), MHD simulations using average solar wind conditions for substorms observed under northward IMF conditions, *J. Geophys. Res. Space Physics*, *120*, 7672–7686, doi:10.1002/2015JA021005.

Peng, Z., C. Wang, Y. F. Yang, H. Li, Y. Q. Hu, and J. Du (2013), Substorms under northward interplanetary magnetic field: Statistical study, *J. Geophys. Res. Space Physics*, *118*, 364–374, doi:10.1029/2012JA018065.

Petrukovich, A. A., W. Baumjohann, R. Nakamura, T. Mukai, and O. A. Troshichev (2000), Small substorms: Solar wind input and magnetotail dynamics, *J. Geophys. Res.*, *105*, 21,109–21,117, doi:10.1029/2000JA900057.

Petrukovich, A. A., W. Baumjohann, R. Nakamura, A. Balogh, T. Mukai, K.-H. Glassmeier, H. Reme, and B. Klecker (2003), Plasma sheet structure during strongly northward IMF, *J. Geophys. Res.*, *108*(A6), 1258, doi:10.1029/2002JA009738.

Pulkkinen, T. I., M. Palmroth, and R. L. McPherron (2007), What drives magnetospheric activity under northward IMF conditions?, *Geophys. Res. Lett.*, *34*, L18104, doi:10.1029/2007GL030619.

Sato, T., and A. Hasegawa (1982), Externally driven magnetic reconnection versus tearing mode instability, *Geophys. Res. Lett.*, *9*, 52–55, doi:10.1029/GL009i001p00052.

Senior, C., J.-C. Cerisier, F. Rich, M. Lester, and G. K. Parks (2002), Strong sunward propagating flow bursts in the night sector during quiet solar wind conditions: SuperDARN and satellite observations, *Ann. Geophys.*, *20*, 771–779, doi:10.5194/angeo-20-771-2002.

Smith, C. W., J. L'Heureux, N. F. Ness, M. H. Acuña, L. F. Burlaga, and J. Scheifele (1998), The ACE magnetic fields experiment, *Space Sci. Rev.*, *86*, 613–632, doi:10.1023/A:1005092216668.

Tang, B. B., C. Wang, Y. Q. Hu, and J. R. Kan (2011), Intensification of the Cowling current in the global MHD simulation model, *J. Geophys. Res.*, *116*, A06204, doi:10.1029/2010JA016320.

Terasawa, T. (1983), Hall current effect on tearing mode instability, *Geophys. Res. Lett.*, *10*, 475–478, doi:10.1029/GL010i006p00475.

Tsurutani, B. T., and W. D. Gonzalez (1995), The efficiency of viscous interaction between the solar wind and the magnetosphere during intense northward IMF events, *Geophys. Res. Lett.*, *22*, 663–666, doi:10.1029/95GL00205.

Wang, C., J. P. Han, H. Li, Z. Peng, and J. D. Richardson (2014), Solar wind-magnetosphere energy coupling function fitting: Results from a global MHD simulation, *J. Geophys. Res. Space Physics*, *119*, 6199–6212, doi:10.1002/2014JA019834.

Wygant, J. R., R. B. Torbert, and F. S. Mozer (1983), Comparison of S3-3 polar cap potential drops with the interplanetary magnetic field and models of magnetopause reconnection, *J. Geophys. Res.*, *88*, 5727–5735, doi:10.1029/JA088iA07p05727.

Zhang, L. Q., Z. X. Liu, Z. W. Ma, W. Baumjohann, Z. Y. Pu, M. W. Dunlop, H. Reme, and J. Y. Wang (2010), X line distribution determined from earthward and tailward convective bursty flows in the central plasma sheet, *J. Geophys. Res.*, *115*, A06218, doi:10.1029/2009JA014429.

Zhang, L. Q., J. Y. Wang, W. Baumjohann, H. Rème, L. Dai, M. W. Dunlop, T. Chen, and Y. Huang (2015a), X-lines in the magnetotail for southward and northward IMF conditions, *J. Geophys. Res. Space Physics*, *120*, 7764–7773, doi:10.1029/2015JA021503.

Zhang, L. Q., A. T. Y. Lui, W. Baumjohann, and J. Y. Wang (2015b), Probabilities of magnetic reconnection encounter as different activity levels in the Earth's magnetotail, *Adv. Space Res.*, *56*, 736–741, doi:10.1016/j.asr.2015.05.001.